Drell-Yan process as an avenue to test a noncommutative standard model at the Large Hadron Collider

Selvaganapathy J,[1,*] Prasanta Kumar Das,[1,†] and Partha Konar[2,‡]

[1]*Department of Physics, Birla Institute of Technology and Science-Pilani, K K Birla Goa campus, Goa 403726, India*

[2]*Physical Research Laboratory, Ahmedabad-380009, India*

(Received 13 February 2016; published 7 June 2016)

We study the Drell-Yan process at the Large Hadron Collider in the presence of the noncommutative extension of the standard model. Using the Seiberg-Witten map, we calculate the production cross section to first order in the noncommutative parameter $\Theta_{\mu\nu}$. Although this idea has been evolving for a long time, only a limited amount of phenomenological analysis has been completed, and this was mostly in the context of the linear collider. An outstanding feature from this nonminimal noncommutative standard model not only modifies the couplings over the SM production channel but also allows additional nonstandard vertices which can play a significant role. Hence, in the Drell-Yan process, as studied in the present analysis, one also needs to account for the gluon fusion process at the tree level. Some of the characteristic signatures, such as oscillatory azimuthal distributions, are an outcome of the momentum-dependent effective couplings. We explore the noncommutative scale $\Lambda_{\rm NC} \geq 0.4$ TeV, considering different machine energy ranging from 7 to 13 TeV.

DOI: 10.1103/PhysRevD.93.116003

I. INTRODUCTION

The Large Hadron Collider (LHC) has so far been extremely successful in discovering and constraining the properties of the last missing bit of the standard model (SM) of particle physics, the Higgs boson [1,2]. Apart from some isolated hints, it is broadly evasive, lacking any clinching evidence yet from physics beyond the standard model (BSM), exploration of which is one of the primary motives for the post-Higgs LHC. On the other hand, it is widely admitted that the SM can at least offer a very good description for low-energy effective theory which, in fact, falls short in explaining several outstanding issues in both theoretical expectations and experimental observations.

The idea of field theories on the noncommutative (NC) spacetime is rather primeval, yet fascinating by introducing a fundamental length scale in the model consistent with the symmetry [3]. These ideas are further revived after realization of their possible connection with the quantum gravity, where noncommutativity is perceived as an outcome of certain string theory embedded into a background magnetic field [4]. Quantum field theory is described by the fields and the local interaction in a continuous spacetime point, where the canonical position and momentum variables x_i, p_j are replaced by the operators $\hat{x}_i$, $\hat{p}_j$ which satisfy the commutation relation

$$[\hat{x}_i, \hat{p}_j] = i\hbar\delta_{ij}.$$

Just like the quantization in phase space, the spacetime coordinate in the noncommutative spacetime gets replaced by an operator $\hat{x}_\mu$ which satisfies the commutation relation

$$[\hat{x}_\mu, \hat{x}_\nu] = i\Theta_{\mu\nu} = i\frac{c_{\mu\nu}}{\Lambda_{\rm NC}^2}, \tag{1}$$

where $\Theta_{\mu\nu}$ is an antisymmetric matrix tensor and of dimension $[M]^{-2}$. Now one can take out the dimension full part in terms of mass parameter $\Lambda_{\rm NC}$ and describe it as the fundamental NC scale at which one expects to see the effect of spacetime noncommutativity. $c_{\mu\nu}$ is the antisymmetric constant c-number matrix which gives a preferred directionality and also a nonvanishing contribution results in deviating from exact Lorentz invariance in some high energy scale $\Lambda_{\rm NC}$. Theoretically, this scale is unknown, but one can try to extract the lower bounds directly from the collider experiments by looking at the characteristic signals this framework can provide. LEP studied the prediction of the process $e^+e^- \to \gamma\gamma$ in the noncommutative QED for several orientations of the OPAL detector and provided the exclusion limit at around 141 GeV [5]. With this very moderate bound, we have the scope for significant improvement at the future runs of the LHC. The Drell-Yan process is arguably the best explored process at the hadron collider. With an extremely clean signal of dilepton, this process is relied upon for calibrating the parton distribution function in hadrons. Any characteristic deviation can easily be a basis for the BSM search. In our present work, we study this important process in the context of the noncommutative framework.

*p2012015@goa.bits-pilani.ac.in
†pdas@goa.bits-pilani.ac.in
‡konar@prl.res.in

There are different approaches to study the effect of spacetime noncommutativity in a field theory. One is the Moyal-Weyl (MW) approach. In this approach, one replaces the ordinary product between two functions $\phi(x)$ and $\psi(x)$ in terms of the $\star$ (Moyal-Weyl) product defined by a formal power series expansion of [6–8]

$$(f \star g)(x) = \exp\left(\frac{1}{2}\Theta_{\mu\nu}\partial_{x^\mu}\partial_{y^\nu}\right) f(x)g(y)|_{y=x}. \quad (2)$$

Here $f(x)$ and $g(x)$ are ordinary functions on R^n, and the expansion in the star product can be seen intuitively as an expansion of the product in its noncommutativity. To describe some of the collider searches of spacetime noncommutativity available in the literature, Hewett *et al.* [9,10] have studied the processes $e^+e^- \to e^+e^-$ (Bhabha) and $e^-e^- \to e^-e^-$ (Moller), and subsequent studies [11,12] were done in the context of $e\gamma \to e\gamma$ (Compton) and $e^+e^- \to \gamma\gamma$ (pair annihilation), $\gamma\gamma \to e^+e^-$ and $\gamma\gamma \to \gamma\gamma$. For a review on NC phenomenology, see [13]. In the context of the LHC, the following investigations are in order. The noncommutative contribution of neutral vector boson (γ, z) pair production was studied [14] at the LHC and the bound was obtained for the NC scale $\Lambda \geq 1$ TeV under some conservative assumptions. Further study on the pair production of charged gauge bosons ($W^\pm$) at the LHC in the noncommutative extension of the standard model found [15] significant deviation of the azimuthal distribution(oscillation) from the SM one (which is a flat distribution) for $\Lambda_{\rm NC} = 700$ GeV. More recently, t-channel single top quark production was calculated at the LHC, and significant deviation in the cross section can be expected from the standard model for $\Lambda_{\rm NC} \geq 980$ GeV [16].

A second way of dealing with this calculation is the Seiberg-Witten approach in which the spacetime noncommutativity is treated perturbatively via the Seiberg-Witten (SW) map expansion of the fields in terms of the noncommutative parameter Θ [4]. Here the gauge parameter λ and the gauge field A^μ are expanded as

$$\lambda_\alpha(x,\Theta) = \alpha(x) + \Theta^{\mu\nu}\lambda^{(1)}_{\mu\nu}(x;\alpha) + \Theta^{\mu\nu}\Theta^{\eta\sigma}\lambda^{(2)}_{\mu\nu\eta\sigma}(x;\alpha) + \cdots \quad (3)$$

$$A_\rho(x,\Theta) = A_\rho(x) + \Theta^{\mu\nu}A^{(1)}_{\mu\nu\rho}(x) + \Theta^{\mu\nu}\Theta^{\eta\sigma}A^{(2)}_{\mu\nu\eta\sigma\rho}(x) + \cdots. \quad (4)$$

The advantage in the SW aprroach over the Weyl-Moyal approach is that it can be applied to any gauge theory, and matter can be in an arbitrary representation. Using this SW map, Calmet *et al.* first constructed [17,18] the *minimal* version of the noncommutative standard model (mNCSM in brief) where they derived the $\mathcal{O}(\Theta)$ Feynman rules of the standard model interactions and found several new interactions which are not present in the standard model. All the above analyses were limited to the leading order in Θ. Phenomenological analysis was carried out for the process $e^+e^- \to \gamma$, $Z \to \mu^+\mu^-$ at the order of Θ^2 and predicted a reach of around $\Lambda_{\rm NC} = 800$ GeV for the NC scale [19,20]. Successive study [21] also focused on the top quark pair production in the NCSM and predicted a similar reach of the NCSM scale.

The noncommutative standard model is essentially the standard model with the background spacetime being noncommutative. Contrary to most other BSM models where particle content and/or the gauge group is extended, there is no new massive degree of freedom included here, but the standard model interactions get modified due to spacetime noncommutativity. This gives rise to the modified standard model interaction vertices extending with additional NC contributions. Moreover, it also provides a host of new vertices which are absent in the SM. It is demonstrated [17,18,22] that the minimal version of NCSM can only be realized in some definite choice of representation for the traces in the gauge field kinetic term. Freedom of this choice leads to a more natural extended version. Melic *et al.* [23,24] formulated the nonminimal version of NCSM (nmNCSM in brief), where the trilinear neutral gauge Boson couplings arise automatically. Note that such anomalous vertices were absent in the minimal version, and the interactions in the fermion sector remain unaffected by different choices of representation in gauge action. Using this formalism, associated Higgs boson production was recently studied associated with the Z boson, taking into account the effect of the Earth's rotation in the nmNCSM. It was found that the azimuthal distribution significantly differs from the standard model result if the NC scale $\Lambda_{\rm NC} \geq 500$ GeV [25].

Exotic new vertices can serve as the Occam's Razor in differentiating the NCSM from other new physics models. In this paper, we discuss this possibility considering one of the very simple but reliable signature at the hadron collider which can portray its ability by distinguishing the effects of spacetime noncommutativity from other new physics scenarios. Our analysis is based on the parton-level Drell-Yan process in producing the lepton pair at the Large Hadron Collider,

$$pp \to l^+l^- + X, \quad (5)$$

where light leptons ($l \equiv e, \mu$) of opposite sign are produced at the final state. What is significant here, besides the standard quark-initiated partonic subprocess for dilepton production, is that gluon-initiated processes can also contribute to this production cross section. In the second process, new triple gauge boson vertices K_{Zgg} and $K_{\gamma gg}$ contribute which arise naturally as an effective vertex in noncommutativity although they are forbidden in the standard model. A study of these vertices has been performed by Behr *et al.* [22]. Using the experimental

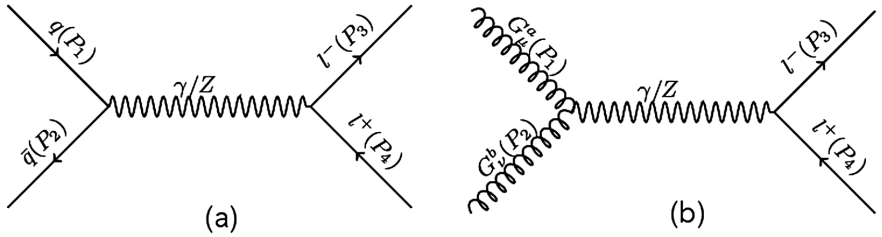

FIG. 1. Representative Feynman diagrams for the partonic subprocess for quark initiated (a) $q\bar{q} \to \gamma, Z \to l^+l^-$, and gluon initiated (b) $gg \to \gamma, Z \to l^+l^-$. Both of them contributes in Drell-Yan type lepton pair production at the hadron collider considering the noncommutative standard model.

LEP upper bound from $\Gamma^{\rm exp}_{Z\to\gamma\gamma} < 1.3 \times 10^{-4}$ GeV and $\Gamma^{\rm exp}_{Z\to gg} < 1.0 \times 10^{-3}$ GeV, a correlated bound on these vertices was obtained for NC scale $\Lambda_{\rm NC} = 1$ TeV.[1]

The organization of the paper is as follows. In Sec. II, we describe the modified vertices and the new set of vertices (found to be absent in the SM) which may potentially contribute to the Drell-Yan lepton pair production at the hadron collider. We next obtain the matrix element square for the partonic subprocess and obtain the total cross section and differential cross section of Drell-Yan lepton pair production. In Sec. III, we demonstrate some of the characteristic distributions, such as lepton pair invariant mass distribution, total cross section, and angular distribution. Arguing in favor of them carrying the hallmark for the noncommutative effects, we probe the sensitivity of the new vertices to the Drell-Yan lepton pair production. Finally, in Sec. IV, we summarize our results and conclude.

II. DRELL-YAN PRODUCTION IN THE NONCOMMUTATIVE STANDARD MODEL

At the LHC, lepton pairs can be produced at the tree level via the (quarklike) parton-initiated process (the only partonic-level processes possible in the SM at the tree level)

$$q\bar{q} \to \gamma, Z \to l^+l^-. \tag{6}$$

In addition, in the NCSM, an additional three boson vertices ensure that lepton pairs can also be produced at the tree level through gluon fusion,

$$gg \to \gamma, Z \to l^+l^-. \tag{7}$$

Representative Feynman diagrams for these partonic subprocess are shown in Fig. 1. For the quark mediated process, the Feynman rules for the vertices $f\bar{f}\gamma$ and $f\bar{f}Z$ (where $f = q, l$) are shown in Appendix A. Note that the vertices, besides the SM part, also contain an extra $\mathcal{O}(\Lambda_{\rm NC})$-dependent term for which, at the limit $\Lambda_{\rm NC} \to \infty$, the original SM vertices get recovered. The second gluon mediated partonic-process comprises two new vertices, γgg and Zgg, which are not present in the SM and are depicted in Fig. 2. Corresponding leading- order Feynman rules in these figures are given by

$$\gamma gg\colon\ (-2e)\sin(2\theta_w)K_{\gamma gg}\theta_3^{\mu\nu\rho}(k_1,k_2,k_3)\delta^{ab} \tag{8}$$

$$Zgg\colon\ (-2e)\sin(2\theta_w)K_{Zgg}\theta_3^{\mu\nu\rho}(k_1,k_2,k_3)\delta^{ab}. \tag{9}$$

Here, θ_W is the Weinberg angle and the vertex factors $K_{\gamma gg}$ and K_{Zgg} are given by

$$K_{\gamma gg} = \frac{-g_s^2}{2gg'}(g'^2+g^2)\zeta_3, \qquad K_{Zgg} = (-\tan\theta_w)K_{\gamma gg},$$

where g_s, g, g' are being the $SU(3)_C$, $SU(2)_L$ and $U(1)_Y$ coupling strengths, respectively. The tensorial quantity[2] $\theta_3 \equiv \theta_3^{\mu\nu\rho}(k_1,k_2,k_3)$ and the parameter ζ_3 are defined in Appendix A. Note that the triple gauge boson vertices K_{Zgg} and $K_{\gamma gg}$, absent in the standard model (once again, one gets a vanishing θ_3 at the limit $\Lambda_{\rm NC} \to \infty$), arise in this nonminimal version of NCSM. A direct test of these vertices have been performed [22] by studying the SM forbidden decays $Z \to \gamma\gamma$ and $Z \to gg$. Analyzing the 3-dimensional simplex that bounds possible values for the coupling constants $K_{\gamma\gamma\gamma}$, $K_{Z\gamma\gamma}$ and K_{Zgg} at the M_Z scale, allowed region for our necessary couplings $(K_{Zgg}, K_{Z\gamma\gamma})$ are obtained as ranging between $(-0.108, -0.340)$ and $(0.217, -0.254)$.

III. RESULT AND DISCUSSION

To estimate the noncommutative effects in our parton-level calculation, we analytically formulate both subprocesses initiated either by a quark-antiquark pair or by a gluon pair at the leading order. Using the Feynman rules to

[1]Note that, in principle, K_{Zgg} (and $K_{\gamma gg}$) can be zero, in combination with two other couplings, $K_{\gamma\gamma\gamma}$ and $K_{Z\gamma\gamma}$. But all three cannot be zero [22] simultaneously, and these other two couplings can be tested at the linear collider with a high degree of precision. We discuss this allowed range in the next section and also demonstrate our results considering different values within this range.

[2]We follow the couplings in similar notation as in [22].

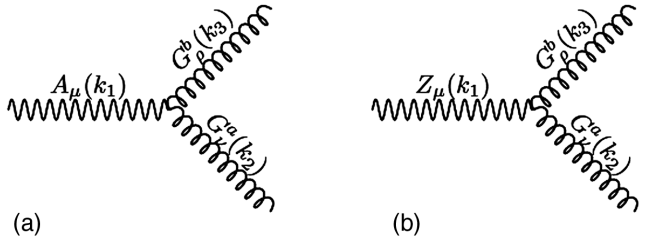

FIG. 2. Feynman diagrams for additional vertices: (a) corresponds to $g-g-\gamma$ vertex, while (b) corresponds to $g-g-Z$ vertex, in the noncommutative standard model which can contribute in Drell-Yan production process at the LHC.

$\mathcal{O}(\Theta)$ as described above and in Appendix A, the squared amplitude (spin-averaged) can be expressed as

$$\overline{|M^2_{\rm NCSM}|}_{ab\to l^+l^-} = \overline{|\mathcal{M}_\gamma + \mathcal{M}_Z|^2} \quad \text{for,} \quad a,b = q,\bar{q} \quad \text{or} \quad g,g. \tag{10}$$

Detailed analytic expression for each nmNCSM amplitude-square is presented in Appendix B. The NC antisymmetric tensor $\Theta_{\mu\nu}$, analogous to the electromagnetic field(photon) strength tensor, has six independent components: three are of the electric type, while three are of the magnetic type. We have chosen $E_i = \frac{1}{\sqrt{3}}$ and $B_i = \frac{1}{\sqrt{3}}$ in our analysis (for more, see Appendix C). We have not considered here the effect of Earth's rotation. The impact of the Earth's rotation on $\Theta_{\mu\nu}$ in the DY process can be interesting and will be investigated in a future work. [26]. Also note that in the DY lepton distribution, besides the Lorentz invariant momentum dot product (e.g. $p_1.p_2$ etc), the Θ-wieghted dot product (e.g. $p_3\Theta p_4$ as one follows from Appendix C) also appears. These terms give rise to nontrivial azimuthal distribution in the Drell-Yan lepton pair production as discussed at the end of our results.

We estimate the parton-level total cross section and differential distributions for the LHC operated at the energy $\sqrt{S}$,

$$d\sigma_{pp\to l^+l^-} = \sum_{ab}\int dx_1 \int dx_2 f_a(x_1,\mu_f^2) f_b(x_2,\mu_f^2) \times d\hat{\sigma}_{ab\to l^+l^-}(x_1x_2S). \tag{11}$$

We employ the CTEQ6L1 parton distribution function (PDF) throughout the analysis, setting the factorization scale μ_f at the dilepton invariant mass M_{ll}. After formulating the setup, we are now in a position to describe the numerical results for the Drell-Yan lepton pair production in the presence of spacetime noncommutativity. In Fig. 3 we have shown the normalized dilepton invariant mass distribution $\frac{1}{\sigma}\frac{d\sigma}{dM_{ll}}$ (GeV^{-1}) against the invariant mass M_{ll} (GeV) corresponding to the LHC machine energy $\sqrt{s}$ at (left plot) 7 TeV and (right plot) 13 TeV. The peak at $M_{ll} = 91.18$ GeV corresponds to the Z boson resonance production. Different continuous curves in both plots correspond to the theoretical (SM and nmNCSM) predictions. Note that the additional positive contributions in nmNCSM curves are realized from two sources: the first being the Θ-dependent NC parts supplemented with the SM vertex, and the second being the complete new tree-level process that enhances significantly. In the 7 TeV (left) plot, the dotted curves correspond to the experimental binwise data provided by the CMS Collaboration [27] for the integrated luminosity 4.5 fb^{-1} and 35.9 pb^{-1} which is presented along with the error bar.

The lowermost curve in each plot (see Fig. 3) is the SM contribution estimated at the leading order. In this figure, we present different NC contributions based on the two relevant parameters $\Lambda_{\rm NC}$ and K_{Zgg} varying between (0.4 TeV–1 TeV) and (−0.108, +0.217), respectively.

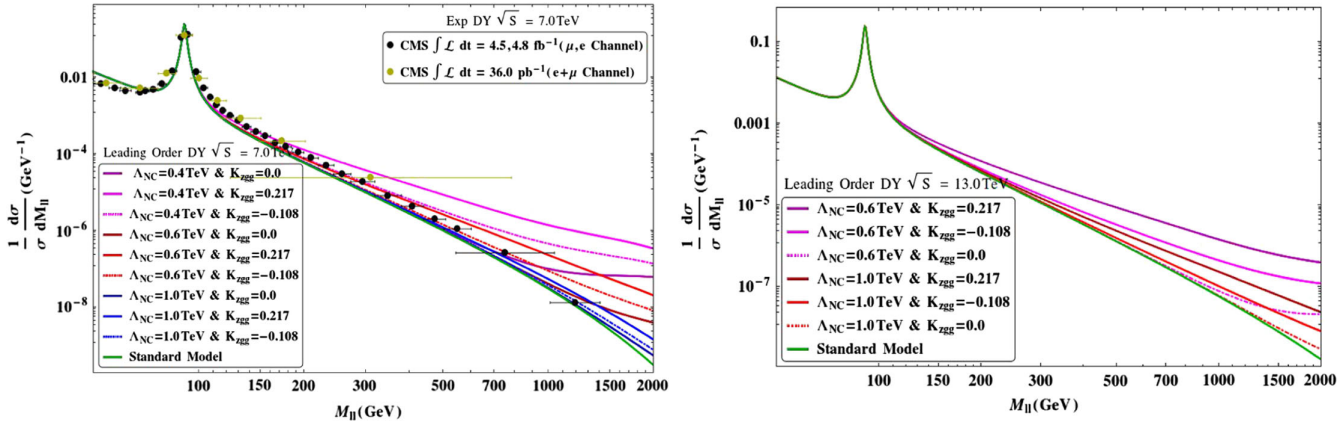

FIG. 3. Normalized invariant mass distribution $\frac{1}{\sigma}\frac{d\sigma}{dM_{ll}}$(GeV^{-1}) as a function of the invariant mass M_{ll} (GeV) is shown corresponding to the machine energy (left plot) $\sqrt{s} = 7$ TeV and (right plot) 13 TeV, respectively. Continuous curves of different colors in both plots are shown for the choice of Λ and K_{Zgg} and they converge to the lowermost SM curve in the limit both of these parameters go to zero. In 7 TeV plot, experimental bin-wise data are also shown with central values and error bars.

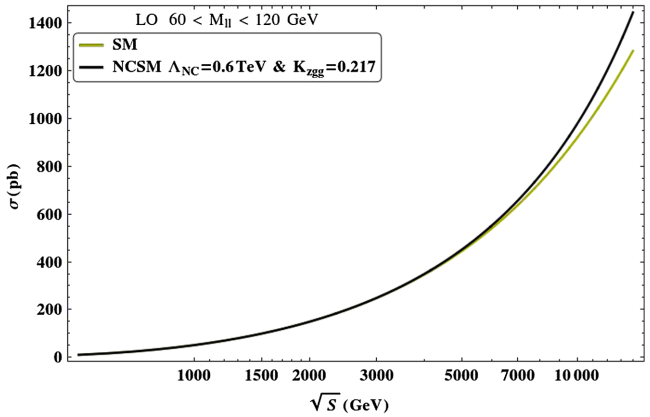

FIG. 4. The Drell-Yan cross section is shown as a function of the LHC machine energy. In the NCSM, we demonstrate with one of the very optimistic choices like $\Lambda_{\rm NC} = 0.6$ TeV and $K_{Zgg} = 0.217$.

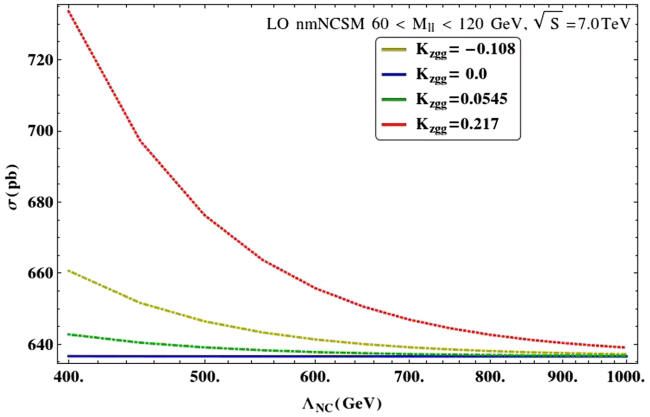

FIG. 5. The total cross section for $pp \to (\gamma, Z) \to l^+l^-$ σ is plotted as a function of the NC scale $\Lambda_{\rm NC}$ (GeV) corresponding to $Z = -0.108$, 0.054 and 0.217 and fixed machine energy $\sqrt{s} = 7.0$ TeV.

Justification for these choices has already been discussed. Note that $K_{Zgg} = 0$ corresponds to the vanishing coupling of the gluon with Z and γ bosons, and the Drell-Yan process in the NCSM arises only from the quark-mediated partonic subprocess $q\bar{q} \to \gamma, Z \to l^+l^-$ as in Fig. 1(a). The NC scale $\Lambda_{\rm NC}$ determines the energy when this BSM effects can be perceived and this phenomena is evident following different scales in the figure. At around a few hundred of dilepton invariant mass, Fig. 3 exhibits, especially at the low $\Lambda_{\rm NC}$ and larger absolute value of K_{Zgg}, the NCSM effect in this distribution deviating from the SM distribution, and it increases with M_{ll}.

In Fig. 4, we have plotted the total leading-order Drell-Yan cross section σ (in pb) against the LHC collision energy $\sqrt{s}$. The lower curve corresponds to the SM cross section. We find $\sigma = 635(1283)$ pb at $\sqrt{s} = 7(14)$ TeV, respectively. To estimate the total cross section, we have considered the dilepton invariant mass interval 60 GeV $< M_{ll} <$ 120 GeV. To visualize the effect we once again consider a very optimistic values of $\Lambda_{\rm NC} = 0.6$ TeV and $K_{Zgg} = 0.217$ for the upper curve corresponds to the NCSM cross section. For reference we present the corresponding Drell-Yan cross sections for different machine energy in Table I. For different machine energy between 7 TeV and 14 TeV, the leading order SM and the nmNCSM (for the same reference parameters) cross sections increases from 636(656) pb to 1283(1438) pb.

In Fig. 5, the nmNCSM Drell-Yan cross section is shown as a function of the NC scale $\Lambda_{\rm NC}$ at a fixed machine energy $\sqrt{s} = 7.0$ TeV. Once again dominant production cross section is estimated for the range of invariant mass 60 GeV $< M_{ll} <$ 120 GeV corresponding to different values of the parameter $K_{Zgg} = -0.108$, 0.0, 0.0545 and 0.217. As expected, for a fixed K_{Zgg} coupling the cross section σ decreases as the NC scale $\Lambda_{\rm NC}$ increases and finally merges to the SM value at the very high value of $\Lambda_{\rm NC}$. Note that the NCSM contribution to DY process for $K_{Zgg} = 0$ almost equal to the SM value as it receives very small contribution from the quark mediated partonic process and the dominant gluon mediated subprocess is absent due to $K_{Zgg} = 0$ (and $K_{\gamma gg} = 0$). That causes this curve as the lowest (almost) horizontal curve, which is hence independent of the $\Lambda_{\rm NC}$ scale. In Table II we present the leading order cross sections estimated for different $\Lambda_{\rm NC} = 0.4$, 0.6 and 1.0 TeV corresponding to $K_{Zgg} = 0$, −0.108 and 0.217.

TABLE I. Drell-Yan cross section in the SM, nmNCSM are shown for 60 GeV $< M_{ll} <$ 120 GeV. The experimental data for the same dilepton invariant mass interval are shown. Here we have set the parameters $\Lambda_{\rm NC} = 0.6$ TeV and $K_{Zgg} = 0.217$ which is optimistic.

	$\sigma_{\rm SM}(pb)$	$\sigma_{nm\rm NCSM}(pb)$	
$\sqrt{S}$ TeV	LO, $\mu_f = M_z$	LO, $\mu_f = M_z$	$\sigma_{\rm EXP}(pb)$
7.0	636	656	974 ± 0.7 (Stat) ± 0.7 (Syst)
8.0	731	760	1138 ± 8 (Stat)
13.0	1193	1325	
14.0	1283	1438	

TABLE II. Drell-Yan cross section $\sigma(pp \to l^+l^-)$ in nmNCSM scenario for the fixed machine energy $\sqrt{s} = 7.0$ TeV. For $K_{Zgg} = 0$, the partonic subprocess $gg \to \gamma, Z \to l^+l^-$ is absent.

Λ_{NC} (TeV)	K_{Zgg}	σ_{NCSM} (pb)	Λ_{NC} (TeV)	K_{Zgg}	σ_{NCSM} (pb)	Λ_{NC} (TeV)	K_{Zgg}	σ_{NCSM} (pb)
0.4	0.0	637	0.6	0.0	637	1.0	0.0	637
0.4	−0.108	661	0.6	−0.108	641	1.0	−0.108	637
0.4	0.217	734	0.6	0.217	656	1.0	0.217	639

After exploring the additional NC contributions coming towards the Drell-Yan production and how different NC parameters can affect such processes, now we would like to point out some of the very characteristic distributions attributed to noncommutativity. Since spacetime noncommutativity essentially breaks the Lorentz invariance, which includes the rotational invariance around beam direction, it can contribute to an anisotropic azimuthal distribution. Angular distributions of the final lepton can thus carry this signature on noncommutativity. Similar feature is noted in many different process earlier related with the NC phenomenology, nevertheless we would like to present this distribution in our context. We show the azimuthal angular distribution for the final lepton in Fig. 6. On the left plot this distribution of the azimuthal angle is shown for Drell-Yan events if the noncommutative effect is there. While the anisotropic effect is not much visible here under the considerably large cross section, it would be evident in the right plot where normalized distribution is demonstrated for that same azimuthal angle. This figure is generated corresponding to different scales $\Lambda_{NC} = 0.6$ TeV and 1 TeV. Also, for each Λ_{NC}, we have selected $K_{Zgg} = -0.108$ and 0.217, respectively.

From the Fig. 6 right plot, we see that the azimuthal distribution of leptons oscillates over ϕ, reaching at their maxima at $\phi = 2.342$ rad and 5.489 rad. The two intermediate minimas are located at $\phi = 0.783$ rad and 3.931 rad. Also note that the azimuthal distribution $\frac{d\sigma}{d\phi}$ is completely flat in the SM. A departure from the flat behavior in the NCSM is due to the term $p_4\Theta p_3(\sim \cos\theta + \sin\theta(\cos\phi + \sin\phi))$ term in the azimuthal distribution which brings ϕ dependence. There still be this feature of azimuthal distribution, even if one deviate from taking the simple form of $\Theta_{\mu\nu}$, however the location of peak positions shift. Such an azimuthal distribution irrespective of peak positions clearly reflects the exclusive nature of spacetime noncommutativity which is rarely to be found in other classes of new physics models and can be tested at LHC.

IV. SUMMARY AND CONCLUSION

The idea that spacetime can become noncommutative at high energy has drawn much attention following the recent advance in string theory. In this paper, we have explored the NC effect in the Drell-Yan lepton pair production $pp \to (\gamma, Z) \to l^+l^-$ at the Large Hadron Collider. Two new vertices, Zgg and γgg, (absent in the SM) are being found to play a crucial role, giving rise to a new partonic subprocess $gg \overset{\gamma,Z}{\to} l^+l^-$ (absent in the SM). For $\sqrt{s} = 7$ TeV, as the coupling parameter K_{Zgg} (corresponding to the new verices Zgg) changes from −0.108 to 0.217, the cross section σ increases from 637(660) pb to 639(734) pb corresponding to $\Lambda_{NC} = 1(0.4)$ TeV. The azimuthal distribution $\frac{d\sigma}{d\phi}$, completely ϕ independent in the SM, deviates substantially in the NCSM. Thus the noncommutative geometry is quite rich in terms of its phenomenological implications, which are worthwhile to explore in the TeV scale Large Hadron Collider.

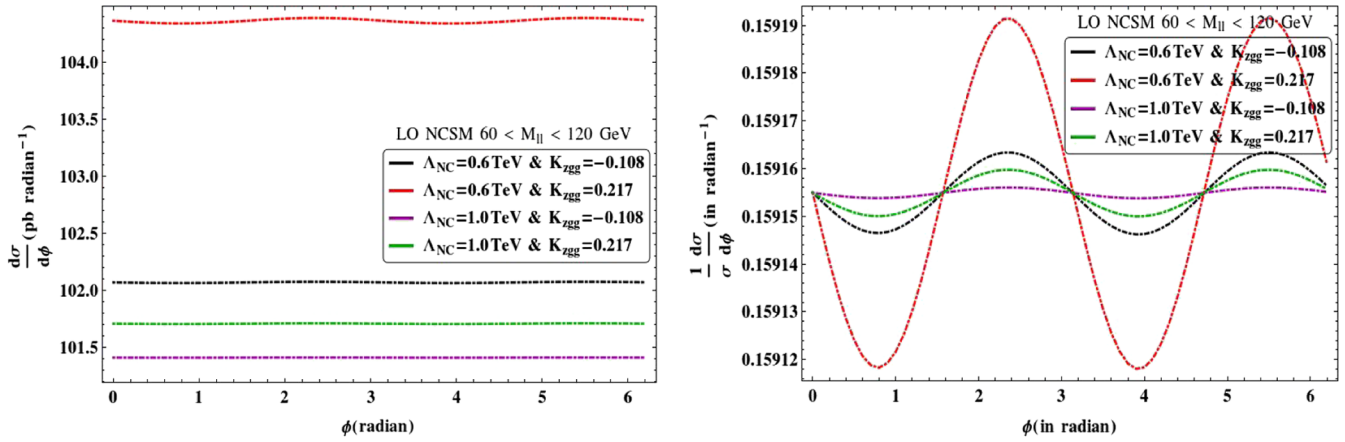

FIG. 6. $\frac{d\sigma}{d\phi}$ as a function of ϕ for $pp \to (\gamma, Z) \to l^+l^-$ $(l = e, \mu)$ for $\Lambda_{NC} = 0.6$ TeV, 1.0 TeV and $K_{Zgg} = -0.108$ and 0.217, respectively.

ACKNOWLEDGMENTS

The work of P. K. Das is supported in parts by the Council of Science and Industrial Research, Government of India, Grant No. 03(1244)12/EMR-II and the Board of Research in Nuclear Science, Department of Atomic Energy, Government of India, Grant No. 2011/37P/08/BRNS. The authors would like to thank Mr. Atanu Guha for useful discussions. Selvaganapathy J would also like to acknowledge his colleague, Mr. Aneesh K. P (recently deceased) for useful discussions.

APPENDIX A: FEYNMAN RULES

The fermion f (quark q and lepton l) coupling to photon and Z bosons, to order $\mathcal{O}(\Theta)$, is given by

$$\gamma f\bar{f}\colon\ ieQ_f\left\{\gamma_\mu+\left[\frac{i}{2}+\left(\frac{P_o\Theta P_i}{8}\right)\right][(P_o\Theta)_\mu(\Delta\not{P}_i)+(\Theta P_i)_\mu(\Delta\not{P}_o)-(P_o\Theta P_i)\gamma_\mu]\right\} \tag{A1}$$

$$\begin{aligned} Zf\bar{f}\colon\ &\frac{ieQ_f}{sin(2\theta_W)}\left\{\gamma_\mu\Gamma_A^-(f)+\left[\frac{i}{2}+\left(\frac{P_o\Theta P_i}{8}\right)\right]\right.\\ &\left.\times[(P_o\Theta)_\mu(\Delta\not{P}_i)\Gamma_A^-(f)+(\Theta P_i)_\mu(\Delta\not{P}_o)\Gamma_A^-(f)-(P_o\Theta P_i)\gamma_\mu\Gamma_A^-(f)]\right\}. \end{aligned} \tag{A2}$$

Here we follow the following notation: i:in, o:out and $\Delta\not{P}_{\text{in,out}}=\not{P}_{\text{in,out}}-m$. Also $\Gamma_A^-(f)=c_V^f-c_A^f\gamma^5$; $c_V^f=I_3^f-2Q_f\sin^2(\theta_W)$; $c_A^f=I_3^f$. Q_f is the e.m. charge, and I_3^f is the third component of the week isospin of the fermion f [quark(q) or lepton(l)].

The factors θ_3 and ζ_3 arise in $\gamma-g-g$ and $Z-g-g$ and are given by [24],

$$\begin{aligned} \theta_3^{\mu\nu\rho}(k_1,k_2,k_3)&=\theta_3[(\mu,k_1),(\nu,k_2),(\rho,k_3)]\\ &=-(k_1\Theta k_2)[(k_1-k_2)^\rho\eta^{\mu\nu}+(k_2-k_3)^\mu\eta^{\nu\rho}+(k_3-k_1)^\nu\eta^{\rho\mu}]\\ &\quad-\Theta^{\mu\nu}[k_1^\rho(k_2\cdot k_3)-k_2^\rho(k_1\cdot k_3)]-\Theta^{\nu\rho}[k_2^\mu(k_3\cdot k_1)-k_3^\mu(k_2\cdot k_1)]\\ &\quad-\Theta^{\rho\mu}[k_3^\nu(k_1\cdot k_2)-k_1^\nu(k_3\cdot k_2)]+(\Theta k_2)^\mu[\eta^{\nu\rho}k_3^2-k_3^\nu k_3^\rho]\\ &\quad+(\Theta k_3)^\mu[\eta^{\nu\rho}k_2^2-k_2^\nu k_2^\rho]+(\Theta k_3)^\nu[\eta^{\mu\rho}k_1^2-k_1^\mu k_1^\rho]+(\Theta k_1)^\nu[\eta^{\mu\rho}k_3^2-k_3^\mu k_3^\rho]\\ &\quad+(\Theta k_1)^\rho[\eta^{\mu\nu}k_2^2-k_2^\mu k_2^\nu]+(\Theta k_2)^\rho[\eta^{\mu\nu}k_1^2-k_1^\mu k_1^\nu], \end{aligned} \tag{A3}$$

and

$$\zeta_3=\frac{1}{3g_3^2}-\frac{1}{6g_4^2}+\frac{1}{6g_5^2}, \tag{A4}$$

where g_3, g_4 and g_5 are the moduli parameters defined in [22].

APPENDIX B: SQUARED-AMPLITUDE TERMS

The amplitude-squared terms for the quark-(anti)quark-initiated partonic subprocess $q\bar{q}\to(\gamma,Z)\to l^+l^-$ from the Feynman diagram 1(a),

$$\overline{|\mathcal{M}_{q,\gamma}|^2}=\left(\frac{AF_1}{3}\right)[(p_1.p_3)(p_2.p_4)+(p_1.p_4)(p_2.p_3)] \tag{B1}$$

$$\begin{aligned} \overline{|\mathcal{M}_{q,Z}|^2}&=\left(\frac{BF_1}{3}\right)(c_A^{l^2}+c_V^{l^2})(c_A^{q^2}+c_V^{q^2})[(p_1.p_3)(p_2.p_4)+(p_1.p_4)(p_2.p_3)]\\ &\quad+\left(\frac{BF_1}{3}\right)c_A^lc_V^lc_A^qc_V^q[(p_1.p_4)(p_2.p_3)-(p_1.p_3)(p_2.p_4)] \end{aligned} \tag{B2}$$

and

$$2\mathrm{Re}\overline{|\mathcal{M}_{q,\gamma}|^{\dagger}|\mathcal{M}_{q,Z}|} = \left(\frac{2CF_1}{3}\right)c_A^l c_A^q[(p_1.p_3)(p_2.p_4)+(p_1.p_4)(p_2.p_3)] - \left(\frac{2CF_1}{3}\right)c_V^l c_V^q[(p_1.p_4)(p_2.p_3)-(p_1.p_3)(p_2.p_4)]. \tag{B3}$$

Here $A=\frac{128\pi^2\alpha^2Q_l^2Q_q^2}{\hat{s}^2}$, $B=\frac{128\pi^2\alpha^2Q_l^2Q_q^2}{\mathrm{Sin}^4 2\theta_W[(\hat{s}-M_z^2)^2+(M_Z\Gamma_Z)^2]}$, $C=\frac{128\pi^2\alpha^2Q_l^2Q_q^2(\hat{s}-M_z^2)}{\hat{s}[(\hat{s}-M_z^2)^2+M_z^2\Gamma_z^2]}$, $F_1=[1+\frac{(P_2\Theta P_1)^2}{4}][1+\frac{(P_4\Theta P_3)^2}{4}]$, and $\hat{s}=sx_1x_2$. Note that amplitude-squared terms go as $\mathcal{O}(1,\frac{1}{\Lambda_{\mathrm{NC}}^2},\frac{1}{\Lambda_{\mathrm{NC}}^4})$, respectively.

For the gluon-initiated partonic subprocess $gg\to(\gamma,Z)\to l^+l^-$, the squared-amplitude terms from the Feynman diagram 1(b) are given by

$$\overline{|\mathcal{M}_{g,\gamma}|^2} = 4DF_2(p_{3\rho}p_{4\sigma}+p_{3\sigma}p_{4\rho}-\eta_{\rho\sigma}p_3\cdot p_4)\cdot(\eta_{\nu\beta}\bar{\theta}_3{}^{\alpha\beta\sigma}\eta_{\alpha\mu}\bar{\theta}_3{}^{\mu\nu\rho}). \tag{B4}$$

Similarly,

$$\overline{|\mathcal{M}_{g,Z}|^2} = 4GF_2(c_A^{l^2}+c_V^{l^2})(p_{3\rho}p_{4\sigma}+p_{3\sigma}p_{4\rho}-\eta_{\rho\sigma}p_3\cdot p_4)(\eta_{\nu\beta}\bar{\theta}_3{}^{\alpha\beta\sigma}\eta_{\alpha\mu}\bar{\theta}_3{}^{\mu\nu\rho}), \tag{B5}$$

$$2\mathrm{Re}\overline{|\mathcal{M}_{g,\gamma}\mathcal{M}_{g,z}^{\dagger}|} = 4HF_2c_V^l(p_{3\rho}p_{4\sigma}+p_{3\sigma}p_{4\rho}-\eta_{\rho\sigma}p_3\cdot p_4)\cdot(\eta_{\nu\beta}\bar{\theta}_3{}^{\alpha\beta\sigma}\eta_{\alpha\mu}\bar{\theta}_3{}^{\mu\nu\rho}), \tag{B6}$$

Here $F_2=[1+\frac{(P_4\Theta P_3)^2}{4}]$, $D=2(\frac{\pi\alpha\sin(2\theta_w)K_{\gamma gg}}{\hat{s}})^2$, $G=[\frac{2\pi^2\alpha^2k_{zgg}^2}{[(\hat{s}-M_z^2)^2+M_z^2\Gamma_z^2]}]$, $H=\sin(2\theta_w)K_{\gamma gg}K_{zgg}[\frac{4\pi^2\alpha^2}{\hat{s}}(\frac{\hat{s}-M_z^2}{[(\hat{s}-M_z^2)^2+M_z^2\Gamma_z^2]})]$. The quantity $\bar{\theta}_3$ appearing in several squared-amplitude terms is given by

$$\bar{\theta}_3^{\mu\nu\rho} = -(p_1\Theta p_2)[(p_1-p_2)^\rho\eta^{\mu\nu}+2(p_2^\mu\eta^{\nu\rho}-p_1^\nu\eta^{\rho\mu})] + (p_1\cdot p_2)[\Theta^{\mu\nu}(p_1-p_2)^\rho-2((p_2\Theta)^\mu\eta^{\nu\rho}+(p_1\Theta)^\nu\eta^{\mu\rho})]+[(p_2\Theta)^\mu p_1^\nu+(p_1\Theta)^\nu p_2^\mu](p_1+p_2)^\rho.$$

Note that amplitude-squared terms go as $\mathcal{O}(\frac{1}{\Lambda_{\mathrm{NC}}^4},\frac{1}{\Lambda_{\mathrm{NC}}^8})$, respectively. In evaluating the matrix element squared, we have used the following orthonormality condition,

$$\sum_{\lambda,\lambda'}\epsilon_{\mu'}^{*a'}(p_1,\lambda_1{}')\epsilon_\mu^a(p_1,\lambda_1) = -\eta_{\mu'\mu}\delta_{a'a} \tag{B7}$$

$$\sum_{\lambda,\lambda'}\epsilon_\nu^b(p_2,\lambda_2)\epsilon_{\nu'}^{*b'}(p_2,\lambda_2{}') = -\eta_{\nu'\nu}\delta_{b'b}, \tag{B8}$$

and the color algebra $\sum_{aa'bb'}\delta_{bb'}\delta_{aa'}\delta^{ab}\delta_{a'b'}=\sum_{ab}\delta^{ab}\delta_{ab}=\sum_{a=1}^{8}\delta_{aa}=8$.

APPENDIX C: ANTISYMMETRIC TENSOR $\Theta_{\mu\nu}$ AND Θ-WEIGHTED DOT PRODUCT

The antisymmetric tensor $\Theta_{\mu\nu}=\frac{1}{\Lambda_{\mathrm{NC}}^2}c_{\mu\nu}$ has six independent components corresponding to $c_{\mu\nu}=(c_{oi},c_{ij})$ with $i,j=1,2,3$. Assuming them to be the nonvanishing components, we can write them as follows:

$$c_{oi}=\xi_i, \qquad c_{ij}=\epsilon_{ijk}\chi^k. \tag{C1}$$

The NC antisymmetric tensor $\Theta_{\mu\nu}$ is analogous to the electromagnetic (e.m.) field strength tensor $F_{\mu\nu}$, and ξ_i and χ_i are like the electric and magnetic field vectors. Setting $\xi_i=(\vec{E})_i=\frac{1}{\sqrt{3}}$ and $\chi_i=(\vec{B})_i=\frac{1}{\sqrt{3}}$ with $i=1,2,3$ and noting the fact that $he\xi_i=-\xi^i$, $\chi_i=-\chi^i$, the normalization condition $\xi_i\xi^j=\frac{1}{3}\delta_i^j$ and $\chi_i\chi^j=\frac{1}{3}\delta_i^j$, we may write $\Theta_{\mu\nu}$ as

$$\Theta_{\mu\nu}=\frac{1}{\sqrt{3}\Lambda_{\mathrm{NC}}^2}\begin{pmatrix}0&1&1&1\\-1&0&-1&1\\-1&1&0&-1\\-1&-1&1&0\end{pmatrix}. \tag{C2}$$

Using these, we may write the Θ-weighted dot product as follows:

$$p_2\Theta p_1=\frac{\hat{s}}{2\sqrt{3}\Lambda_{\mathrm{NC}}^2} \tag{C3}$$

$$p_4\Theta p_3=\frac{\hat{s}}{2\sqrt{3}\Lambda_{\mathrm{NC}}^2}[\cos\theta+\sin\theta(\cos\phi+\sin\phi)]. \tag{C4}$$

Here we have not considered the effect of the Earth's rotation on the antisymmetric tensor $\Theta_{\mu\nu}$ in the DY process. This will be reported elsewhere [26].

[1] S. Chatrchyan *et al.* (CMS Collaboration), Observation of a new boson at a mass of 125 GeV with the CMS experiment at the LHC, Phys. Lett. B **716**, 30 (2012).
[2] G. Aad *et al.* (ATLAS Collaboration), Observation of a new particle in the search for the Standard Model Higgs boson with the ATLAS detector at the LHC, Phys. Lett. B **716**, 1 (2012).
[3] H. S. Snyder, Quantized Space-Time, Phys. Rev. **71**, 38 (1947).
[4] N. Seiberg and E. Witten, String theory and noncommutative geometry, J. High Energy Phys. 09 (1999) 032.
[5] OPAL Collaboration, Test of non-commutative QED in the process $e^+e^- \to \gamma\gamma$ at LEP, Phys. Lett. B **568**, 181 (2003).
[6] I. F. Riad and M. M. Sheikh-Jabbari, On Moyal-Weyl map, J. High Energy Phys. 08 (2000) 045.
[7] B. Jurco and P. Schupp, Noncommutative Yang-Mills from equivalence of star products, Eur. Phys. J. C **14**, 367 (2000).
[8] J. M. Gracia-Bondia and J. C. Varilly, Quantum electrodynamics in external fields from the spin representation, J. Math. Phys. (N.Y.) **35**, 3340 (1994).
[9] J. Hewett, F. J. Petriello, and T. G. Rizzo, in Signals for noncommutative QED at high energy e^+e^- colliders, eConf C010630, E3064 (2001).
[10] J. L. Hewett, F. J. Petriello, and T. G. Rizzo, Signals for noncommutative interactions at linear colliders, Phys. Rev. D **64**, 075012 (2001).
[11] P. Mathews, Compton scattering in noncommutative space-time at the NLC, Phys. Rev. D **63**, 075007 (2001).
[12] T. G. Rizzo, QED at future e^+e^- colliders, Int. J. Mod. Phys. A **18**, 2797 (2003).
[13] I. Hinchliffe, N. Kersting, and Y. L. Ma, Review of the phenomenology of noncommutative geometry, Int. J. Mod. Phys. A **19**, 179 (2004).
[14] A. Alboteanu, T. Ohl, and R. Ruckl, Probing the noncommutative standard model at hadron colliders, Phys. Rev. D **74**, 096004 (2006).
[15] T. Ohl and C. Speckner, The noncommutative standard model and polarization in charged gauge boson production at the LHC, Phys. Rev. D **82**, 116011 (2010).
[16] S. Y. Ayazi, S. Esmaeili, and M. M. Najafabadi, Single top quark production in t-channel at the LHC in noncommutative space-time, Phys. Lett. B **712**, 93 (2012).
[17] X. Calmet, B. Jurco, P. Schupp, J. Wess, and M. Wohlgenannt, The standard model on noncommutative spacetime, Eur. Phys. J. C **23**, 363 (2002).
[18] X. Calmet and M. Wohlgenannt, Effective field theories on noncommutative space-time, Phys. Rev. D **68**, 025016 (2003).
[19] A. Prakash, A. Mitra, and P. K. Das, $e^-e^+ \to \mu^-\mu^+$ scattering in the NCSM, Phys. Rev. D **82**, 055020 (2010).
[20] A. Prakash and P. K. Das, Laboratory frame analysis of $e^-e^+ \to \mu^-\mu^+$ scattering in the noncommutative standard model, Int. J. Mod. Phys. A **27**, 1250141 (2012).
[21] R. S. Manohar, J. Selvaganapathy, and P. K. Das, Probing spacetime noncommutativity in the top quark pair production at e^+e^- collider, Int. J. Mod. Phys. A **29**, 1450156 (2014).
[22] W. Behr, N. G. Deshpande, G. Duplancic, P. Schupp, J. Trampetic, and J. Wess, The $Z \to \gamma\gamma$, gg decays in the noncommutative standard model, Eur. Phys. J. C **29**, 441 (2003).
[23] B. Melić, K. P. Kumericki, J. Trampetic, P. Schupp, and M. Wohlgenannt, The standard model on non-commutative space-time: Electroweak currents and Higgs sector, Eur. Phys. J. C **42**, 483 (2005).
[24] B. Melić, K. Passek-Kumerički, J. Trampetić, P. Schupp, and M. Wohlgenannt, The standard model on non-commutative space-time: Strong interaction included, Eur. Phys. J. C **42**, 499 (2005).
[25] J. Selvaganapathy, Prasanta Kr. Das, and Partha Konar, Search for associated production of Higgs with Z boson in the noncommutative standard model at linear colliders, Int. J. Mod. Phys. A **30**, 155015 (2015).
[26] J. Selvaganapathy, A. Guha, P. Konar, and P. K. Das (to be published).
[27] CMS Collaboration, Measurement of the Drell-Yan cross section in pp collisions at $\sqrt{s} = 7$ TeV, J. High Energy Phys. 10 (2011) 007; arXiv:1108.0566.